

Modulated adiabatic passage of oriented nuclei. II. Experimental results for CoFe alloys

P. J. Back and D. H. Chaplin

*Department of Physics, University College, The University of New South Wales,
Australian Defence Force Academy, Canberra, Australian Capital Territory 2600, Australia*

P. T. Callaghan

Department of Physics and Biophysics, Massey University, Palmerston North, New Zealand

(Received 28 April 1987)

The new technique of modulated adiabatic passage on oriented nuclei (MAPON) is shown to provide self-consistent signs and magnitudes for the principal component of the electric-field-gradient tensor at ^{60}Co and ^{58}Co nuclei in single-crystal iron. The best result for the mode value is $V_{ZZ} = +3.4(5) \times 10^{19}$ V/m². A further test of MAPON using ^{56}Co in single-crystal iron yields a quadrupole moment of $Q_{56} = +25(9)$ fm², in excellent agreement with systematics and theory. Experimentally derived distributions in electric field gradients are found to be consistent with sample-preparation procedures. These results firmly establish MAPON as capable of resolving extremely fine features in the electronic charge distribution at nuclear probes and with the wide applicability and sensitivity of nuclear-magnetic-resonance spectroscopy on oriented nuclei.

I. INTRODUCTION

It is the purpose of this paper to demonstrate through self-consistent measurements that modulated adiabatic passage of oriented nuclei (MAPON) provides detailed knowledge on the magnitude, sign, and distribution of the electric field gradients (EFG's) at light to intermediate-mass nuclei in nominally cubic ferromagnets. By comparison with single passage, the approach does not necessarily demand knowledge of the rf field at the nuclei, nor require the statistically demanding time resolution of midpassage signals (MPS).¹ No detailed curve fitting of the raw data is required once the effects of the spin-lattice relaxation and inhomogeneous broadening on the basic MAPON signals presented in the previous paper² (to be referred to as I) are understood. Furthermore, it is shown that gross inhomogeneous broadening is not a fundamental limitation of the technique.

In order to establish the credentials of MAPON we have chosen a series of cobalt isotopes separately diffused into single-crystal iron hosts. Only those results which impinge on establishing MAPON are presented here; further results, in particular, the precision measurement of the EFG as a function of principal crystal directions will be presented in a later publication.

A preliminary MAPON experiment to deduce the sign, mode magnitude, and distribution of the electric quadrupole interaction (EQI) at ^{60}Co in single-crystal iron has been published previously.³ Encouraging agreement was obtained between P/h and the earlier single-passage result of Callaghan *et al.*^{4,5} for the same system, where P is defined by Eq. (7) in I. Noting, however, the inherent difficulties of analysis of single-passage NMR ON data, it was necessary to seek further confirmation of the $^{60}\text{CoFe}$ MAPON result. In particular, the sign and magnitude of the impurity EFG for CoFe is independently measured by MAPON using ^{58}Co , whose quadrupole moment is

known with comparable accuracy to that of ^{60}Co . A further MAPON study is made using ^{56}Co , prepared primarily as part of a concurrent NMR ON spin-echo program, but with the additional aim to determine its quadrupole moment using the deduced EFG from MAPON measurements on the other Co isotopes; agreement with systematics or calculation would serve as a final self-consistent check on MAPON. The spin-echo program is linked to the present study both in the investigation of nuclear spin-spin relaxation and the associated question of a spin temperature, and in the modification of the spin-echo decay through the quadrupole interaction. As noted in I, the latter is the subject of future work.

II. EXPERIMENTAL

A. Samples

$^{58}\text{CoFe}$. The $^{58}\text{CoFe}$ sample was prepared using an iron single-crystal from Kristallhandel Kelpin (Leimen, F.R.G.) cut in the (110) face as a 9-mm-diameter, 1-mm-thick disk. A 5-mm disk was spark cut from the center and polished to 1 μm , first with 600 paper and followed by diamond paste and etched lightly in 0.1M HNO₃. The activity was carrier-free ^{58}Co deposited by micropipette at the center of the disk. The activity was diffused at 830°C for 30 mins under flowing hydrogen at one atmosphere pressure. After loading, the sample was allowed to cool at about 10°C per min. Subsequent etches in 0.1M HNO₃ removed 75% of the activity. The average cobalt concentration within the diffusion depth of ~ 0.5 μm was estimated to be 0.001 at. %.

$^{56}\text{CoFe}$. This iron single crystal was obtained from a different source, as a 3.5-mm diameter, 0.6-mm-thick disk. The surface was etched in dilute nitric acid, diamond polished to 1 μm , and loaded with ~ 180 μCi of carrier-free ^{56}Co . Diffusing for 15 mins at 830°C again

under flowing hydrogen led to $\sim 10\%$ loss of activity to the surrounding crucible and vitreous silica tube, and a further 48% loss by repeated wiping with cotton buds soaked in distilled water. Cobalt concentration was of the order 0.001 at. %. An earlier weaker ^{56}Co sample using an iron single-crystal host from the same batch yielded well-resolved midpassage structure in single passage,⁶ indicating a well-defined EFG.

$^{60}\text{CoFe}$. The sample preparation has been described earlier.³ The iron single crystal was from the same batch as the $^{56}\text{CoFe}$ samples. A notable feature of this relatively highly concentrated (0.03 at. % ^{60}Co ; 0.6 at. % $^{60}\text{Co} + ^{59}\text{Co}$) sample, prepared for parallel and detailed NMRON spin-echo studies, was its inability to yield time-resolved midpassage signals in single passage. Although some midpassage structure was just discernable, the EFG was clearly not as well defined as the earlier, much more dilute sample prepared by Callaghan *et al.*⁴

B. Cryogenic assembly

In all three experiments the single-crystal disk samples were oriented to $\pm 2^\circ$ using Laue back-reflection x-ray photographs and mounted in an adiabatic demagnetization cryostat with the [001] (magnetically easy) axis in the (110) plane of the disk parallel to both the γ -ray detector and the polarizing field. The samples were cooled to between 10 and 15 mK using a 250-g chrome-alum-salt pill. In all cases these samples were subjected to magnetic fields of up to 6 T along the easy axis prior to and during the cooling process. In this way large working anisotropies were achieved in zero magnetic field, once the sample was cooled. In the case of the earlier $^{56}\text{CoFe}$ the zero-field γ -ray anisotropy equalled the saturating high-field anisotropy, indicating almost perfect alignment of domains along the [001] direction in the plane of the sample. For $^{56}\text{CoFe}$ and $^{60}\text{CoFe}$ spin-echo NMRON measurements were undertaken, often with the same cryogenic assembly.

An important requirement for adiabatic passage is that T_1 and T_2 relaxation times be much greater than the time taken to sweep the natural linewidth γB_1 . In our experiments this transit time is less than 1 ms, many orders of magnitude less than T_1 , and considerably less than the spin-spin relaxation times for ^{60}Co and ^{56}Co in these single-crystal iron samples. The spin-spin relaxation times, as measured by the irreversible decay of the spin echoes, were comparable and of order 50 ms, about one order of magnitude slower than the previously published result⁷ for ^{60}Co in polycrystalline iron. The $^{58}\text{CoFe}$ resonant frequency of ~ 440 MHz is too high for the rf power amplifiers in our spin-echo apparatus.

C. MAPON methodology

In the preceding paper MAPON was described as a development from single-passage NMRON. For modulation frequencies which greatly exceed the quadrupole splitting the modulated passage can be viewed in terms of the successive single passages of two rf fields. In the vicinity of the MAPON "effect" where the modulation fre-

quency is comparable with the splitting, the passage comprises a succession of pseudo-spin-1 subresonances. This leads to a final population distribution, prior to spin-lattice relaxation, that depends on the direction of sweep, and more importantly, on the frequency separation of the two rf fields relative to the EQI subresonance splitting.

General expressions for the nuclear hyperfine Hamiltonian and the electric quadrupole interaction are given by Eq. (7) of I. In this experimental paper, however, cyclic frequencies are used except where reference is made to the preceding paper. We focus our attention on the subresonance separation $2P/h$, where the quadrupole splitting factor P is given by Eq. (8) of I. For the purposes of this paper we assume that the EFG is parallel to the dominant magnetic axis (i.e., $\alpha=0$, so that $V_{zz}=V_{ZZ}$), and possesses axial symmetry, so that the asymmetry parameter $\eta=0$. Additional measurements are required to test these assumptions. However, in this work only the nuclear probe is varied, and the EFG symmetry axis in each sample should possess a common orientation.

In I the responses of MAPON passages were calculated as a function of f_m for different spins and rf conditions. The results may be summarized as follows: (a) A clear difference is found in the NMRON postpassage signal (PPS) depending on whether the rf sideband splitting of $2f_m$ exceeds or is less than $2P/h$, and a marked inflection is obtained in the region $2f_m \sim 2P/h$ of the MAPON spectrum. (b) The point of inflection experiences a small shift to lower frequency by an amount of order $\frac{1}{2}\gamma\bar{k}_m B_1/2\pi$, where B_1 is the circularly polarized rf amplitude at the nucleus and \bar{k}_m as given in I is of the order 2 to 4 for the cases analyzed here. (c) While the magnitude of the PPS is dependent on the adiabatic parameter A [Eq. (28) of I], it is not necessary to measure or fit this quantity in order to find P/h . Relatively low levels of applied rf field were initially employed so that consideration (b) was not of great consequence.

The experiment to determine P/h consists of measuring the NMRON PPS as a function of f_m . Again, the γ -ray distribution $W(\theta)$ is given by

$$W(\theta) = \sum_v B_v U_v F_v P_v (\cos\theta) \quad (1)$$

with terms as defined in I. The NMRON signal ΔW is the relative destruction of thermal equilibrium anisotropy $[1 - W_{\text{TE}}(0)]$, defined by

$$\Delta W = (W_{\text{rf}} - W_{\text{TE}})/(1 - W_{\text{TE}}) \times 100\% \quad (2)$$

It is necessary to consider the effects of spin-lattice relaxation (SLR) during transit through the inhomogeneously broadened line. For most practical systems the SLR strongly modifies the form of the ideal signals seen in I. This is due to finite sweep times through the inhomogeneously broadened line. Less fundamentally, the practice of obtaining experimental signals $\Delta W(t)$, as an integral count over a time window should this represent a significant fraction of the SLR, further modifies the MA-

PON theoretical signals of I. Note that this relaxation occurs on a time scale much larger than that required for transit of one isochromat and does not affect the adiabaticity. Our detailed line-shape calculations refer to $^{58}\text{CoFe}$ since this system yields the largest and best defined EQI and furthermore demonstrates the general advantages of MAPON over single passage. For each value of f_m the time-dependent signal $\Delta W(t)$ was found by applying the $2j + 2$ successive subresonance operators $|U_{mn}|^2$ to the spin ensemble [see Eq. (25) of I], starting from thermal equilibrium. Relaxation is incorporated during and after the passage according to a "master equation"⁸

$$\frac{d\rho_m}{dt} = \sum_{m'} (W_{m'm}\rho_{m'} - W_{mm'}\rho_m), \quad (3)$$

where ρ_m is the population of the nuclear substate $|m\rangle$.

The transition probabilities $W_{m'm}$ were obtained from a relaxation constant $C_K = 0.108 \text{ s K}$ as appropriate for $^{58}\text{CoFe}$ [001] in zero external field.⁹ In Fig. 1 the relaxation curve $\Delta W(t)$ is shown with and without broadening at fixed $f_m > P/h$. At time t_p immediately following the passage through an isochromat large signals are predicted, for first entering the most populated or least populated levels [$\Delta W(t_p) = -150\%$ or $+700\%$, respectively]. However, for $t > t_p$ the signal rapidly changes due to SLR. This large transient signal is further obscured by broadening, also shown in Fig. 1, in which $\Delta W(t)$ is con-

volved over a presumed Gaussian line shape. In Fig. 2 the "integral" MAPON spectrum $\Delta W(t_p)$ is shown for a range of modulation frequencies centered on P/h for (a) ideal case, i.e., without relaxation, and (b) counting a finite time following a passage which includes SLR and broadening. Figure 2(b) mirrors typical experimental conditions of a 2-s window measured after completion of the rf sweep. Clearly the form of the spectra is modified due to SLR and broadening, the magnitude and sign of the changes reflecting similar variations to those obtained with single passage.¹ In particular the signal for entering the most populated level with $f_m > P/h$ has changed sign so that the integral spectra for the two sweep directions are now similar in form. Nevertheless, the positions and widths of the transition regions are not altered by more than of order $\gamma B_1/2\pi$ in frequency, so that the observations (a)–(c) for the ideal spectra still apply. Similar considerations and conclusions apply to $^{56,60}\text{CoFe}$.

It is instructive to compare the above MAPON considerations with those for time-resolved MPS in single passage NMR ON. ^{60}Co is a more suitable case for time resolution since the structure of the unbroadened MPS is constant within 30% throughout the $2j$ population interchanges. This enables P/h to be extracted from the MPS in samples for which the inhomogeneous broadening Δf is as great as $(2j - 1)2P/h$. By contrast, for ^{58}Co , the nuclear decay coefficients U_2F_2 and U_4F_4 are of opposite sign which produces rapid fluctuations in the sign and

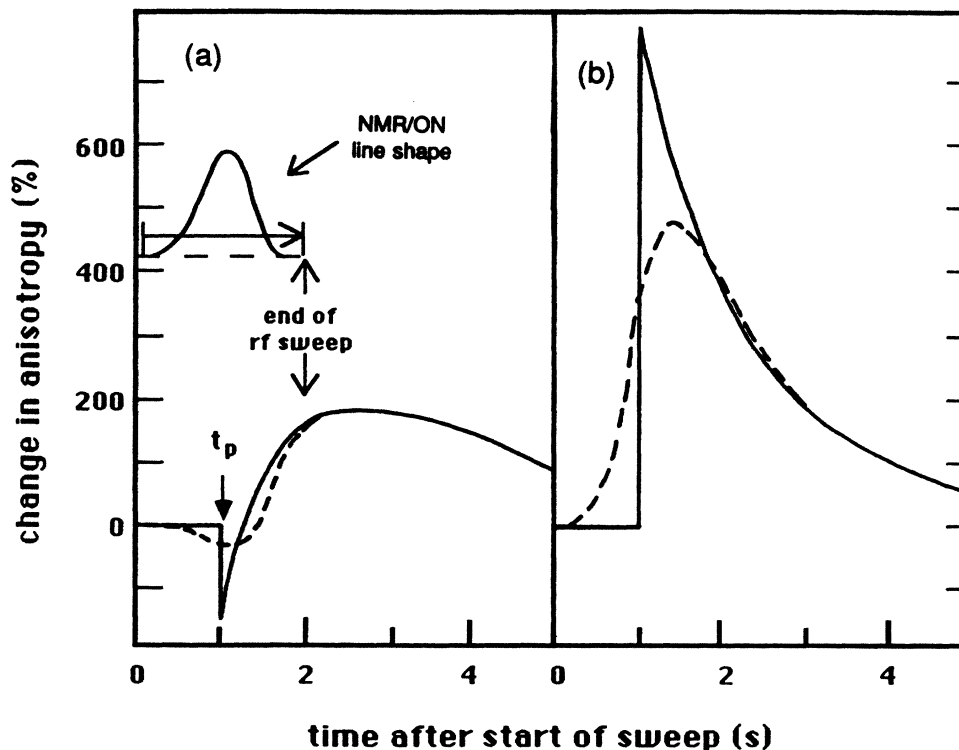


FIG. 1. Theoretical postpassage signals (PPS) for $^{58}\text{CoFe}$ following a MAPON sweep for fixed $f_m > P/h$. Curves are for first entering (a) most populated, (b) least populated quadrupolar split subresonances. Solid curves are for an isochromat with $P/h = 25 \text{ kHz}$; t_p defines the end of the MAPON passage. For clarity the structure of the rapidly oscillating midpassage signal (MPS) up to t_p is omitted. The dashed curves include inhomogeneous broadening of 800 kHz ; $T = 12.5 \text{ mK}$, $A = 8.0$, $C_K = 0.108 \text{ s K}$ (see text and Ref. 9).

magnitude of ΔW during the passage. This more complex structure is sensitive to Δf of the order $2P/h$. The time resolution of the ^{58}Co MPS is thus impeded despite the larger value of the spectroscopic quadrupole moment.

We may thus make important distinctions between MAPON and single passage, in that the MAPON signal for selected f_m is obtained by observing postpassage signals, which are usually much more slowly varying functions of time than the midpassage signals, and consequently far less sensitive to broadening. Furthermore the analysis of the MPS requires a detailed and quantitative

fit of the time dependence of the γ -ray anisotropy and is dependent upon a knowledge of the exact distribution of rf fields. This necessity is obviated by MAPON whereby one need only observe a change in PPS resulting from a change in modulation frequency.

D. MAPON electronics

Experimentally the MAPON sweep depicted in Fig. 4 of I is achieved by amplitude modulating a swept rf carrier, of frequency f_c , using a double-balanced mixer, as shown in Fig. 3. This produces a double-sideband, suppressed carrier, with rf components $f_c \pm f_m$, sweeping with fixed frequency separation $2f_m$. The audio modulating frequency f_m is derived from a programmable function generator. In the present experimental study the amplitudes of the carrier component f_c and spurious harmonics at $f_c \pm n f_m$ were more than 34 dB below the principal sidebands in the present apparatus. The adiabatic parameter associated with these spurious components was thus so small that their contributions to the resonant signals were negligible. Of greater importance is the spectral purity of the two principal sidebands. This is limited largely by spectral noise in the rf generator, and incidental FM signals entering via the sweep circuitry. In the present study the full width at half maximum of each

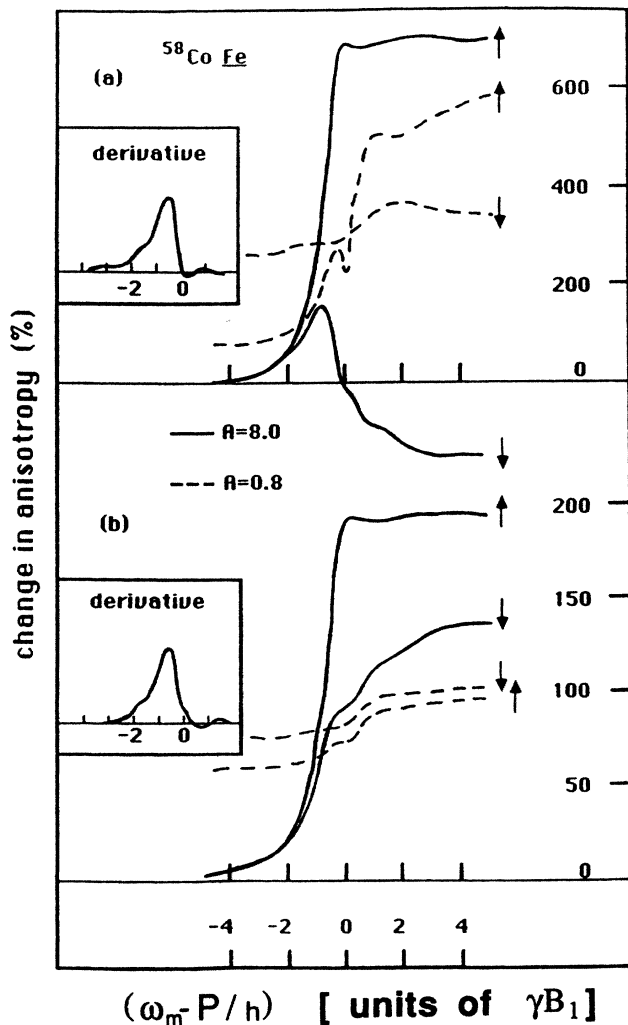


FIG. 2. Theoretical "integral" MAPON spectra measured from PPS relaxation curves from a range of modulation frequencies. Curves are for (a) ideal MAPON signals prior to SLR and without broadening, (b) practical MAPON signals consisting of 2-s windows for inhomogeneously broadened resonances. The count is commenced on completion of entire sweep. Curves are labeled for entering the most populated quadrupolar subresonance first (\downarrow), or for entering least populated first (\uparrow). Note the greatly reduced sweep asymmetry of the practical MAPON signals, particularly for small A . The abscissae are dimensioned in units of rf field γB_1 , thereby directly demonstrating the shift to lower frequencies of the MAPON inflection. Insets: The "differential" spectra for $A=8.0$, and forward sweep (\uparrow).

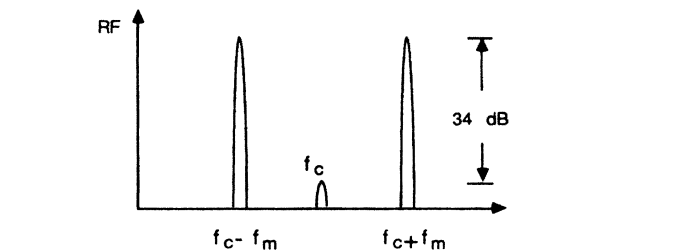
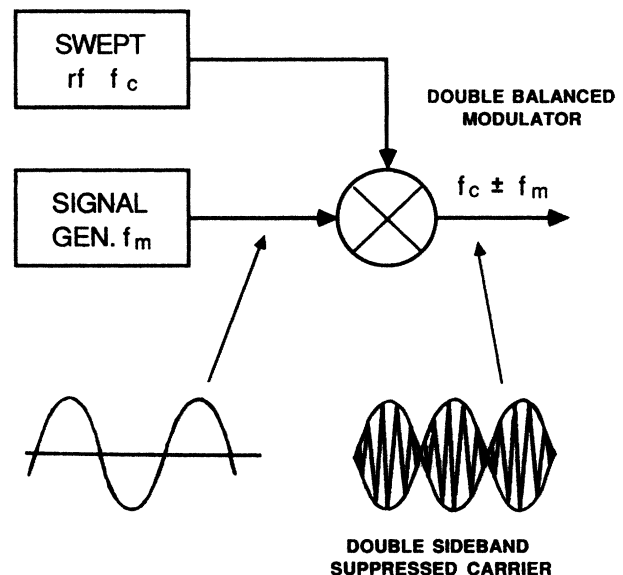


FIG. 3. Generation of swept rf pair for MAPON experiment, using double sideband, suppressed carrier modulation of the linearly swept rf carrier.

sideband was less than 200 Hz, which restricted the lowest f_m for sensible MAPON population interchanges to ~ 500 Hz. Care is required to monitor and preserve the fidelity of the rf sidebands used in MAPON (and single carrier in single-passage experiments), as spurious incidental FM signals will lead to subsaturation population equalization and not the required cyclic permutations.¹⁰

III. RESULTS

A. ⁵⁸CoFe

The "magnetization" curve for this sample is plotted in Fig. 4(a) as $W(\theta)$ versus polarizing field B_{pol} . This was measured for decreasing B_{pol} . In the region $B_{\text{pol}} \sim 0.4 \rightarrow 0.3$ T the anisotropy $[1 - W(\theta)]\%$ decreases from its saturation value $[1 - W(0)] = 16\%$ during domain nucleation, increasing again in lower field. The zero-field anisotropy corresponds to 75% alignment of domains along that [001] easy axis which is aligned in the plane of the sample and parallel to the detector direction, assuming the remainder are along the other two [001]

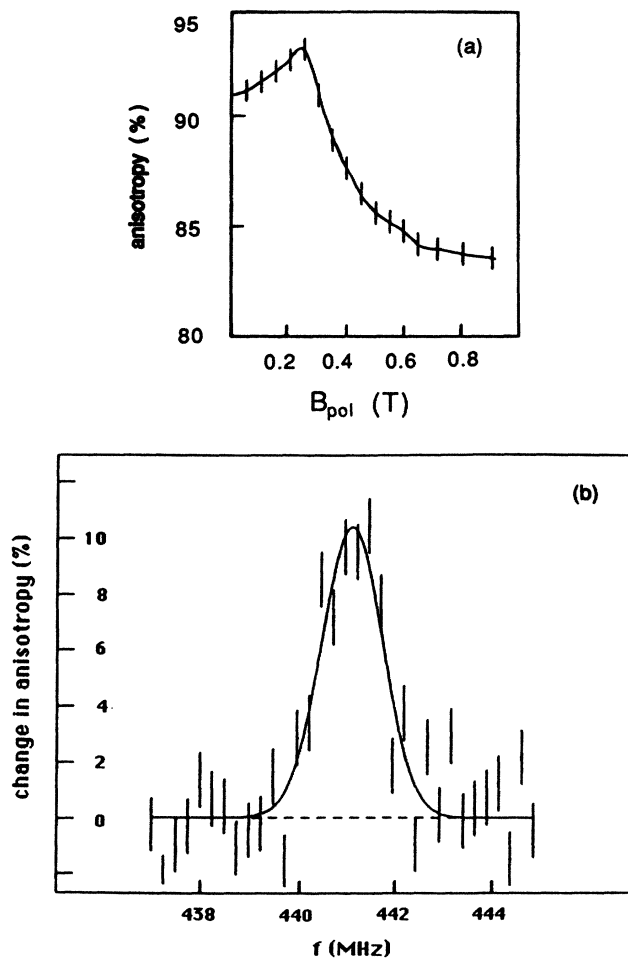


FIG. 4. (a) "Magnetization" curve for ⁵⁸CoFe; γ -ray anisotropy $[1 - W(\theta)]\%$ measured in decreasing field along [001]. (b) Zero-field cw NMR ON resonance for above sample using $\Delta f = \pm 500$ kHz.

axes. The zero-field cw NMR ON line shape in Fig. 4(b) indicates a central resonance at 441.3(2) MHz with a full width at half maximum of 1.2 MHz, which includes 0.2 MHz modulation broadening. Due to loss of enhancement factor the saturation field resonance could not be obtained without significant rf heating.

Preliminary single-passage measurements were performed to detect the presence of the quadrupole interaction and to try to observe any midpassage structure. Figure 5 shows the time-dependent anisotropy upon sweeping through the zero-field resonance. The postpassage asymmetry due to quadrupole splitting^{1,5} is evident and indicates that the sign of P is positive. However, the midpassage structure is obscured, and this precludes the possibility of extracting the magnitude of P using unmodulated single passage.

The raw MAPON "sweep profiles" for both sweep directions, measured from the commencement of the modulated passage, are shown in Fig. 6(a), using the same rf parameters as in Fig. 5, with $f_m = 50$ kHz. The sweep direction asymmetry is clearly evident, due to the greater changes in B_v 's produced by the passage of the 2 rf sidebands, for $f_m > P/h$. With the same rf parameters, but setting $f_m = 500$ Hz, a remarkable absence of signal following the passage is observed [Fig. 6(b)]. This results from the almost complete reversal of each subsaturation population inversion by the second rf sideband, as expected for $f_m < P/h$. For these experiments the applied field was zero. For saturating fields the contrast between $f_m < P/h$ and $f_m > P/h$ was less well pronounced due to the reduction in effective adiabatic parameter and technical complications due to the rf heating.

The "integral" MAPON spectrum is now obtained by recording ΔW , measured as a 2-s count following a 2-MHz sweep up, as a function of f_m . In Fig. 7 ΔW is almost zero at low frequencies, rising to above 60% at the highest modulation frequencies, consistent with the previous calculations. The parameter P/h is found directly from this curve by differentiation. The result, as seen in Fig. 8, is a broad spectrum, with mode value and full width at half maximum (FWHM) given by

$$P_m/h = 23(1) \text{ kHz}$$

and

$$(P/h)_{\text{FWHM}} = 12 \text{ kHz}.$$

For the purpose of discussion the adiabatic parameter was estimated by inspection of the sweep profiles. The relative form of the postpassage relaxation curves for the two sweep directions is approximated by selecting $A = 4.0$ and $P > 0$, as shown by the solid curves in Fig. 6(a). A complete calculation would include the attenuation of the rf field within the sample, as was done for single passage.¹ From this value of A the effective experimental linewidth $\frac{1}{2}\gamma\bar{k}_m B_1/2\pi$ (Sec. III B of I) is estimated to be of the order 900 Hz. Clearly the experimental data are dominated by broadening of the EQI, and the rf field makes little contribution to this result, either to the width or the mode value for ⁵⁸CoFe. Attempts to observe the effect of the rf field at higher power were prevented by rf heating.

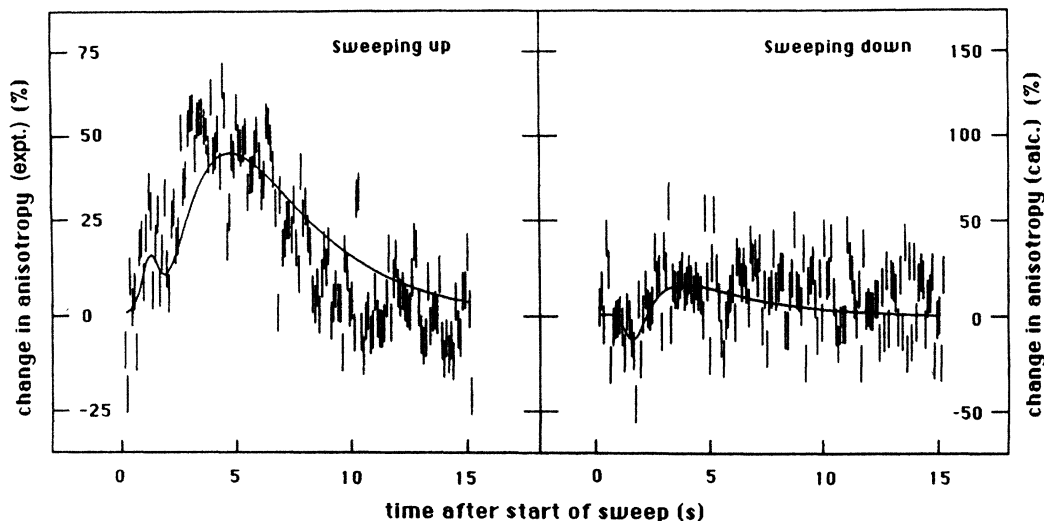


FIG. 5. Single-passage sweeps for $^{58}\text{CoFe}$. Note the complete absence of MPS as a result of the broadening. $1/T=80\text{ K}^{-1}$, $B_{\text{pol}}=0\text{ T}$, sweep 2 MHz in 2 s . The solid lines are calculated for sweeping through a broadened resonance of 800 kHz , assuming $A=4.0$, P positive, $C_K=0.108\text{ s K}$.

A high-field (0.7 T) MAPON spectrum was obtained for comparison. Due to loss of rf enhancement, the corrections to mode values are of even less significance. Because of the better definition of P_m/h and well-defined direction of the magnetic hyperfine field for the magnetically saturated host, we take as our best value for V_{ZZ} for CoFe the high field ^{58}Co result $V_{ZZ}=+3.4(5)\times 10^{19}\text{ V/m}^2$.

B. $^{60}\text{CoFe}$

A zero-field MAPON spectrum for $^{60}\text{CoFe}$ [001] is also shown in Fig. 8 for comparison, the results being

$$P_m/h = +4.5(10)\text{ kHz}$$

(uncorrected for rf field shift)

and

$$(P/h)_{\text{FWHM}} = 5\text{ kHz}.$$

Again the MAPON response reflects broadening of the EQI. In this sample a high-frequency tail is seen, extending to nearly 40 kHz . The zero-field spectrum is very similar to the 0.3-T result published previously³ for the same sample. A 2.0-T spectrum containing fewer data due to increased warming of the salt pill, led to a less accurate but consistent result of

$$P_m/h = +7.0(20)\text{ kHz}$$

and

$$(P/h)_{\text{FWHM}} = 6\text{ kHz}.$$

From the mode values of these results V_{ZZ} can be found using Eq. (7) of I, and these are summarized in Table I. The zero-field mode values for $^{60}\text{CoFe}$ are also

depressed by the rf field strength by about 1 kHz as determined from 90° pulses using pulsed NMR ON, but the table entries are uncorrected values read directly from the inflection of the MAPON response. It is clear that the signs and magnitudes of the electric field gradients are consistent between the two isotopes and the magnitudes the same, within the accuracy of the data, in zero and saturating magnetic fields. The bias to lower values for V_{ZZ} for $^{60}\text{CoFe}$ almost certainly reflects an effective rf field $\frac{1}{2}k_m B_1$ somewhat larger than in the $^{58}\text{CoFe}$ experiments.

C. $^{56}\text{CoFe}$

MAPON measurements using $^{56}\text{CoFe}$ [001] also yield a sweep asymmetry corresponding to a positive P . The integral and differential spectra are shown in Fig. 9 for $d|\omega|/dt > 0$. These data indicate a broad distribution described by

$$P_m/h = +5.8(10)\text{ kHz}$$

and

$$(P/h)_{\text{FWHM}} = 5\text{ kHz}.$$

The distribution of P/h , as for $^{60}\text{CoFe}$, is characterized by a high-frequency tail, but extending only to 25 kHz . The electric quadrupole moment of the ground state of ^{56}Co may now be obtained from Eq. (7) of I using the best value of V_{ZZ} [$3.4(5)\times 10^{19}\text{ V/m}^2$]. We use the high-field result of this sample together with that of $^{58}\text{CoFe}$ to give

$$Q_{56}/Q_{58} = +1.13(34)$$

and using $Q_{58} = +22(3)\text{ fm}^2$ (Ref. 11) we have

$$Q_{56} = +25(9)\text{ fm}^2.$$

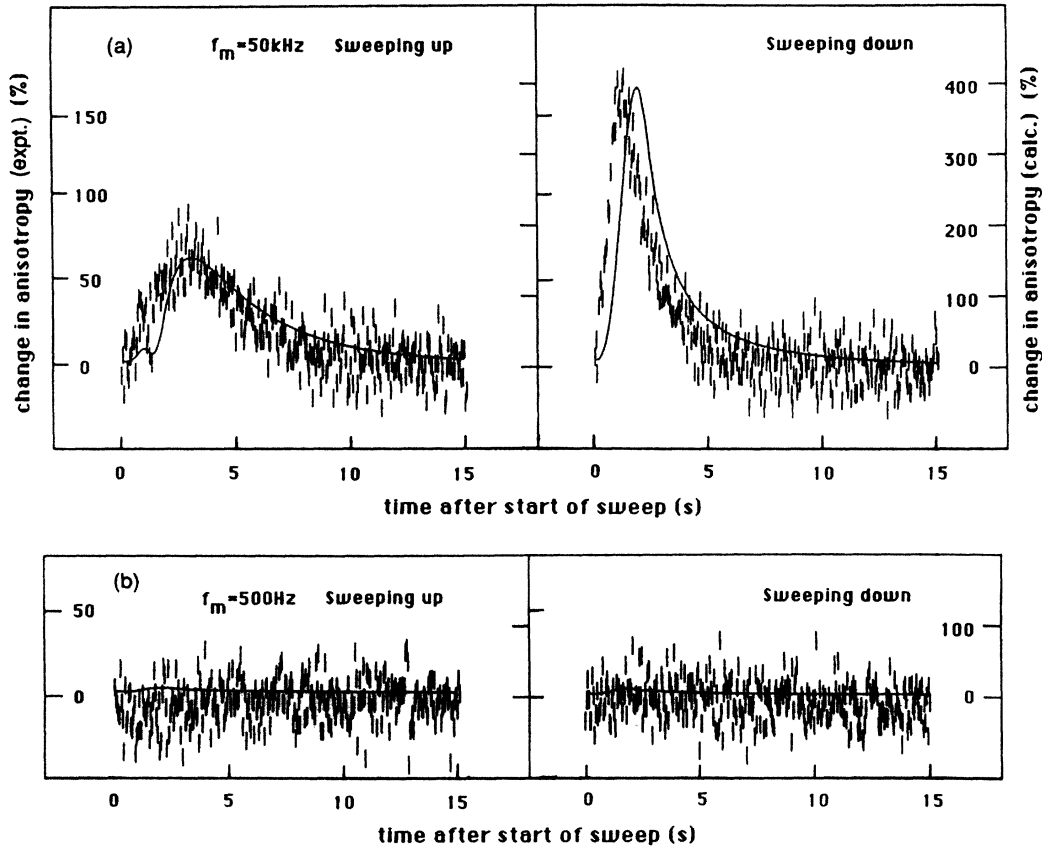


FIG. 6. MAPON sweep for $^{58}\text{CoFe}$ for fixed f_m using the same peak-to-peak rf amplitude as in Fig. 5. (a) $f_m = 50 \text{ kHz}$; (b) $f_m = 500 \text{ Hz}$. $1/T = 80 \text{ K}^{-1}$, $B_{\text{pol}} = 0 \text{ T}$, sweep 2 MHz in 2 s . The solid curves were calculated as in Fig. 5 assuming $P/h = 25 \text{ kHz}$.

This value is in excellent agreement with the microscopic shell-model calculation¹² which predicts $Q_{56} = +25 \text{ fm}^2$.

IV. DISCUSSION

The experimental investigation has sought primarily to test the general applicability of the MAPON technique in extracting a weak electric quadrupole splitting in the presence of a much larger Larmor frequency and inhomogeneous broadening. Consistent results for the CoFe impurity EFG have been obtained using ^{58}Co and ^{60}Co over a range of rf excitation conditions.

EFG distributions from all three samples have broadly similar characteristics, with full widths at half maxima of 50–100% of the mode value. The widths in the P distributions are of the order 10–20 times the intrinsic MAPON linewidth. The ^{56}Co and ^{60}Co results each have a high-frequency tail extending to several times the mode value, which is not apparent in the more symmetrical ^{58}Co result. We believe this feature, in part, arises from additional strain-induced EFG's¹³ in the ^{56}Co and ^{60}Co host disks. The ^{58}Co host was spark cut from the central region of a much larger disk, and peripheral strain would have been removed. The more extensive distribution in the $^{60}\text{CoFe}$ spectrum compared with $^{56}\text{CoFe}$ may indicate a contribution from nearest-neighbor Co atoms. It has been noted in (3) that a satellite cw NMRON resonance

was observed in this sample, arising from the high- ^{59}Co carrier concentration ($>95\%$) in the ^{60}Co activity. By contrast carrier-free ^{56}Co and ^{58}Co were used in the present study. The differing distributions, therefore, appear to reflect additional broadening of the EQI in the ^{60}Co sample, indicating that the MAPON technique can provide detailed information on the distribution, as well as the sign and magnitude of V_{zz} . Further work with codiffused samples is required to verify this aspect.

The ^{58}Co result is particularly encouraging, since this system is not amenable to single-passage MPS analysis, even when the distribution of rf fields is known over the diffusion profile. In fact the relaxation curves for both single and modulated passage were reproduced by assuming that only 40% of the ^{58}Co nuclei are resonated. This is not surprising, as the rf skin depth at 440 MHz is only about $0.5 \mu\text{m}$, which is comparable with the diffusion depth of the activity. Furthermore, the total quadrupolar-split resonance width $(2j-1)2P/h$ ($\sim 200 \text{ kHz}$) is less than 20% of the inhomogeneously broadened linewidth in this sample, and the possibility of observing a statistically significant differential resonance displacement¹⁴ is diminished by the lower γ -ray anisotropy and faster spin-lattice relaxation. Despite these problems the MAPON technique has proven highly effective for this system, a result which supports the suggestion that MAPON is a spectroscopic tool, depending on the details of

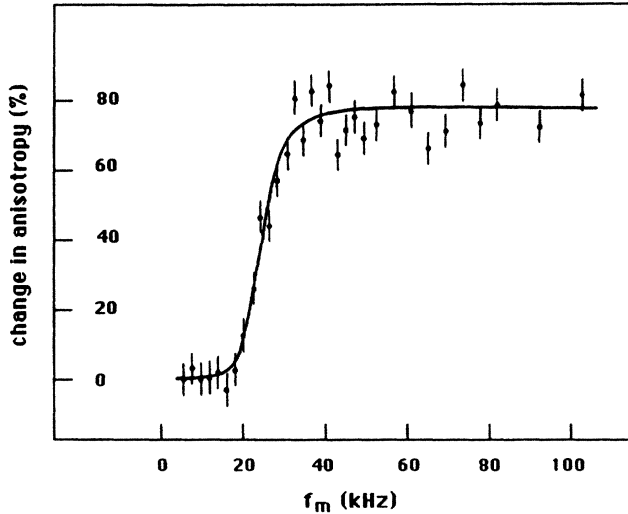


FIG. 7. MAPON "integral" spectrum for $^{58}\text{CoFe}$. Each point is the result of 50 individual sweeps, the time window being taken as the first 2 s of the postpassage signal for sweep up. To minimize the effect of baseline drift the frequency f_m was stepped after each individual MAPON sweep. Experimental conditions as for Fig. 6.

the rf frequency but not its magnitude.

The measurement of P/h for $^{56}\text{CoFe}$ yields a quadrupole moment $Q_{56} = +25(9) \text{ fm}^2$ that is in accord with systematics and calculation. The ground-state nucleus is isobaric with and only one proton deficient from the doubly magic ^{56}Ni core nucleus. Quadrupole moments are, therefore, likely to be small, certainly less than 50 fm^2 . The addition of two neutrons to form ^{58}Co is not likely to significantly alter the quadrupole moment since, within the independent coupling scheme of the $j-j$ shell model, these neutrons should pair off leaving the quadrupole moment essentially determined by the proton configuration

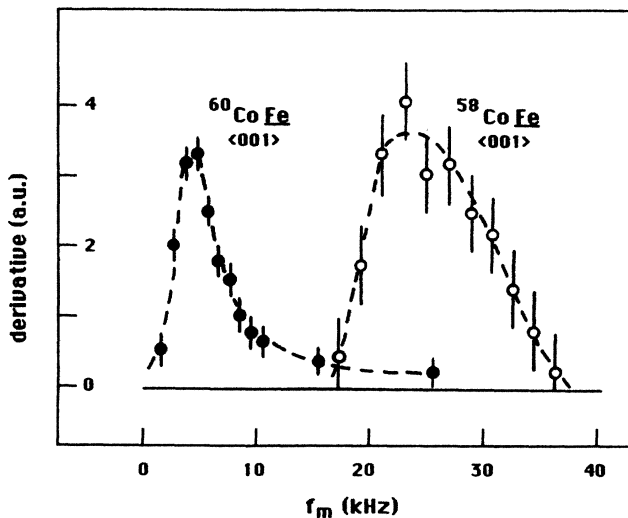


FIG. 8. Distribution of P/h for $^{58}\text{CoFe}$ for $B_{\text{pol}}=0 \text{ T}$ obtained by differentiating the best-fit curve for data in Fig. 7. Also shown is the zero-field result for $^{60}\text{CoFe}$. The extensive high-frequency tail on the $^{60}\text{CoFe}$ data is not apparent in the $^{58}\text{CoFe}$ data, as discussed in the text.

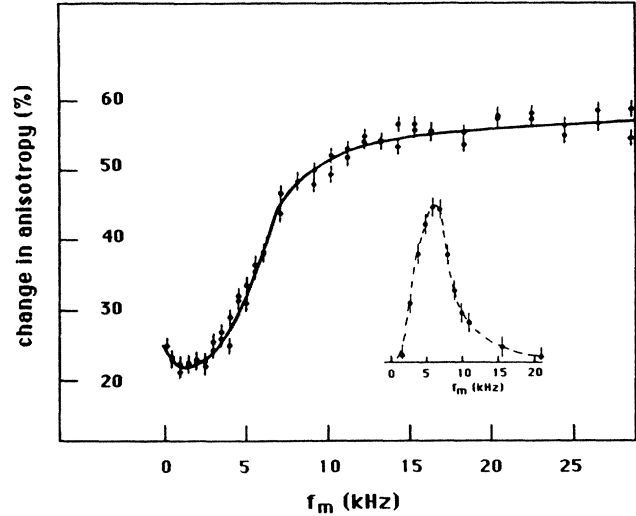


FIG. 9. $^{56}\text{CoFe}$ MAPON "integral" spectrum for $B_{\text{pol}}=0 \text{ T}$. Inset: The distribution of P/h , obtained by differentiation.

of the ^{56}Co nucleus. Thus the best estimate for Q_{56} based on known experimental values is that for ^{58}Co , namely, $+22(3) \text{ fm}^2$. Note that irrespective of whether the Q_{58} value becomes superseded the MAPON result predicts a similar valued Q_{56} . In addition, the shell-model calculations of Mooy and Glaudemans¹² leading to $Q_{56} = +25 \text{ fm}^2$ incorporate a larger than usual configuration space with no imposed restrictions on configuration mixing. Their calculations are remarkably successful in predicting excitation energies, g -factors, and quadrupole moments for all nuclei in the mass range $A=52-60$. In particular they calculate $Q_{58} = +26 \text{ fm}^2$ in close agreement with the experimental value of $+22(3) \text{ fm}^2$.

These considerations give us confidence in proceeding with further, more accurate MAPON measurements of the EFG and for other crystal directions. A full discussion of the EFG orientation dependence is deferred until these measurements are completed. However, some points are noted here, for the $[001]$ crystal direction.

The observation of gross sweep asymmetry in single passage and MAPON points immediately to an EFG that is predominantly unique in magnitude and sign. Such an EFG, spin orbit in origin, is well established for the heavy impurities Ir and Au.¹ Comparison of the EFG distribution for $^{58}\text{CoFe}$ with the less well-defined EFG's

TABLE I. Experimental values for the EQI and associated electric field gradient for CoFe as measured by MAPON.

	P/h (kHz)	V_{ZZ} (10^{19} V/m^2)
	Zero field	
^{58}Co	$+23.0(10)$	$+3.5(5)$
^{60}Co	$+4.5(10)$	$+2.5(6)$
	Saturating fields	
^{58}Co (0.7 T)	$+22.5(20)$	$+3.4(5)$
^{60}Co (0.3 T)	$+4.5(10)$	$+2.5(6)$
(2.0 T)	$+7.0(20)$	$+3.9(5)$

for $^{60}\text{CoFe}$ and $^{56}\text{CoFe}$, after due allowance for the different quadrupole moments, suggests that there probably is an underlying, essentially unique V_{ZZ} . This is, however, sufficiently small in CoFe alloys that random contributions arising from impurities and defects, which vary from sample to sample, can significantly compete in determining the electrostatic energy of nuclear orientation. Note that for the integral spin systems studied here, there is no concern with the absence of first-order quadrupolar broadening in the $\frac{1}{2} \rightarrow -\frac{1}{2}$ substate transition of the $\frac{1}{2}$ integral spin systems which may lead to an erroneous interpretation of the extent of broadening. The origin of the unique component can, for single-crystal studies, be spontaneous magnetostriction, local-moment spin-orbit coupling, or both.

The constancy of the MAPON response between zero field and saturating field along the [001] direction is interesting. It is tempting to immediately reject magnetostriction as an important mechanism since the mode value does not change with field. Suppose, however, in zero field, the magnetostrictive strain axis is solely along the [001] detector direction because of the magnetic prehistory. For an unmagnetized single crystal we expect preferential domain alignment along the easy [001] axes and similar alignment of the impurity magnetic hyperfine fields, assuming these are parallel to the domain magnetization. The integral anisotropy "magnetization curves" for both $^{58}\text{CoFe}$ and $^{60}\text{CoFe}$ provide at most for 25% and 12%, respectively, of nuclei in zero-applied magnetic field to be along the two orthogonal [001] axes, where α , if 0° for the detector axis, is now 90° . Although $P_2(\cos\alpha)$ changes sign and halves in magnitude for these nuclei, it is doubtful whether the total effect of so few nuclei would have been easily discernable at our current level of accuracy for determining P_m/h . The geometry of these domain nuclei is such that the rf field is more likely to move their domain walls than reach the active nuclei,

tending to exclude them from the MAPON signal observed in zero field. Indeed the very large zero-field anisotropy and the form of the integral anisotropy magnetization curves suggest, respectively, predominant zero-field alignment of the domains along the [001] detector axis and predominant 180° wall displacement during the magnetization process. Under these conditions the bulk magnetostriction is nearly fully developed in zero field, and so the characteristic signature of increasing strain with magnetization is heavily diluted.

Alternatively, should the minority orthogonal [001] domains in zero field possess a well-defined magnetostrictive principal axis parallel to their magnetization, then $\alpha=0^\circ$ for all domain nuclei. The zero-field and high-field limits for the EFG would be indistinguishable, no matter what fraction experience the resonant rf fields, as is the case for the spin-orbit mechanism. In principle very careful MAPON experiments at intermediate fields along [001], or more sensibly, at saturating fields along other crystal directions could distinguish between the two mechanisms. They might also yield values for the EFG asymmetry parameter when the sample is magnetized along, for example, the [110] axis.

In summary, the experiments performed to date do not preclude magnetostriction as a significant contribution to the EFG in CoFe alloys although the spin-orbit local-moment contribution is more readily reconcilable with the field insensitivity of the mode values.

ACKNOWLEDGMENTS

The authors are grateful to Dr. D. C. Creagh for helpful discussions on aspects of the Laue x-ray analysis and Dr. H. R. Foster for assistance with the early experiments. We also acknowledge valuable discussions with Professor B. G. Turrell. This project is supported by the Australian Research Grants Scheme.

¹N. J. Stone, *Hyperfine Int.* **8**, 83 (1980).

²P. T. Callaghan, P. J. Back, and D. H. Chaplin (preceding paper) *Phys. Rev. B* **37**, 4900 (1988).

³P. T. Callaghan, P. J. Back, D. H. Chaplin, H. R. Foster, and G. V. H. Wilson, *Hyperfine Int.* **22**, 39 (1985).

⁴P. T. Callaghan, W. M. Lattimer, N. J. Stone, and P. D. Johnston, *Hyperfine Int.* **2**, 291 (1976).

⁵W. M. Lattimer, Ph.D. thesis, Oxford University, 1976.

⁶P. J. Back, D. H. Chaplin, H. R. Foster, G. A. Stewart, and G. V. H. Wilson, *Hyperfine Int.* **22**, 193 (1985).

⁷H. R. Foster, P. Cooke, D. H. Chaplin, P. Lynam, D. E. Swan, and G. V. H. Wilson, *Hyperfine Int.* **4**, 357 (1978).

⁸See, for example, E. Klein, in *Low-Temperature Nuclear Orientation*, edited by N. J. Stone and H. Postma (Elsevier, Amsterdam, 1986), Chap. 12.

⁹The relaxation constant for single-crystal iron is a very strong function of applied field and crystal orientation. The high-

field value for CoFe from M. Kopp and E. Klein, *Hyperfine Int.* **11**, 153 (1981) was scaled to zero field according to the single-crystal $^{131}\text{I}Fe$ results of H. D. Rüter, W. Haaks, E. W. Duczinski, E. Gerdau, D. Visser, and L. Niesen, *Hyperfine Int.* **9**, 385 (1981). The results would indicate that this value $C_K=0.108$ s K is an overestimate for our $^{58}\text{CoFe}$ sample. See, in particular, Fig. 6(a).

¹⁰P. T. Callaghan, P. D. Johnston, and N. J. Stone, *J. Phys. C* **7**, 3161 (1974).

¹¹*Table of Isotopes*, 7th ed., edited by C. M. Lederer and V. S. Shirley (Wiley, New York, 1978).

¹²A. B. M. Mooy and P. W. M. Glaudemans, *Z. Phys. A* **312**, 59 (1983).

¹³R. C. Mercader and T. E. Cranshaw, *J. Phys. F* **5**, L124 (1975).

¹⁴E. Hagn, *Phys. Rev. B* **25**, 1521 (1982); E. Hagn and E. Zech, *ibid.* **25**, 1529 (1982).